Arabian Journal for Science and Engineering (2020) 45:4967–4974
https://doi.org/10.1007/s13369-020-04576-6

RESEARCH ARTICLE-PHYSICS

First Principle Insight into the Structural, Optoelectronic, Half Metallic, and Mechanical Properties of Cubic Perovskite $NdInO_3$

Mehwish K. Butt[1] · Muhammad Yaseen[1] · Abdul Ghaffar[1] · Muhammad Zahid[2]

Received: 30 December 2019 / Accepted: 24 April 2020 / Published online: 8 May 2020

Abstract
The structural, optoelectronic, magnetic, and elastic properties of cubic perovskite $NdInO_3$ have been analyzed by spin-polarized density functional theory. The computed values of total energies of the optimized systems reveal that ferromagnetic phase is energetically stable rather than paramagnetic phase of cubic $NdInO_3$ compound. Furthermore, the spin-polarized band structure and density of states elucidate the half metallic nature of the studied material due to a different response of both spin channels; spin-up electrons illustrate metallic character, while spin-down electrons display a direct band gap (M–M) semiconducting behavior. The elastic parameters indicate anisotropic and brittle characteristics; further, the total magnetic moment of the cubic $NdInO_3$ perovskite (3 μB) is mainly due to the Nd site with very feeble contribution of In and O atoms. The complete set of optical parameters demonstrate that cubic $NdInO_3$ is active in visible–ultraviolet region. Based on these results, $NdInO_3$ is categorized as a half metallic ferromagnetic compound, which might be used in spintronics and optoelectronic devices.

Keywords DFT · Half metallic ferromagnetism · Optical properties · Elastic properties

1 Introduction

Half metallic ferromagnetic materials (HMFM) have been of core interest since their discovery in 1983 [1]. These materials are very important due to their usage in tunnel junctions [2], extremely effectual magnetic sensors [3], and magnetic devices [4]. Furthermore, HMFM also play a crucial role in spintronics, because they exhibit metallic behavior in one spin channel and semiconducting or insulating characteristics in another spin channel which results in 100% spin polarization around the Fermi level [5, 6]. Meanwhile, perovskites have also attracted researchers of the modern era due to some unique properties such as colossal magneto resistance [7], ferromagnetism [8, 9], and high-temperature superconductivity [8], which make these compounds a candidate of technological and industrial applications including transducers, solar cells, optoelectronics, memory devices, and spintronics [10–13].

Lanthanides-based cubic perovskites are interesting members of the half metallic ferromagnetic family. In a recent study, cubic $NdGaO_3$ is found to be a half metallic ferromagnet. Hybridization between O-2*p* and Nd-4*f* orbitals is responsible for the possible origin of ferromagnetism [14]. Similarly, different other compounds like $PrMnO_3$ [15], double perovskites A_2FeMO_6 (M = Mo, Re, and W) [16], binary compounds like ZnSe (V doped) [17], GeTe (Cr doped), and ZnTe (Cr and Mn doped) [18], perovskite alloys such as Sr_2FeMoO_6 [19], and $La0.7Sr_{0.3}MnO_3$ [20] have been studied theoretically to disclose their half metallic ferromagnetic nature by DFT. In addition, Rashid et al. [21] studied the electromagnetic and thermoelectric properties of XVO_3 (X = Ba, La) compounds using first principle calculations and declared these materials as half metallic ferromagnets. Sandeep et al. [22] theoretically determined the magneto-electronic properties of $EuAlO_3$ and predicted its half metallic nature. Moreover, Dan Li et al. [23] evaluated the change in structural and optoelectronic properties of rhombohedral $NdAlO_3$ as a result of pressure variations, and Yang et al. [24] analyzed the optical and structural properties of $0.5NdAlO_3$–$0.5CaTiO_3$ by DFT.

✉ Muhammad Yaseen
myaseen_taha@yahoo.com; m.yaseen@uaf.edu.pk

[1] Department of Physics, University of Agriculture, Faisalabad 38040, Pakistan

[2] Department of Chemistry, University of Agriculture, Faisalabad 38040, Pakistan

In this work, structural, optoelectronic, magnetic, and elastic properties of cubic $NdInO_3$ compound have been investigated by using highly precise density functional theory using the PBE-GGA functional. It is observed that this compound in its cubic phase shows half metallic ferromagnetism. To our knowledge, there are no data regarding the electronic, elastic, optical, and magnetic properties of cubic phase of $NdInO_3$ compound, which has motivated us to explore this material. These results may pave a path for implementation of this material in spintronics.

2 Computational Details

In this study, we used the WIEN2k DFT code that uses full potential linearized augmented plan wave method (FP-LAPW) [25]. We used it to evaluate the total energies and electronic, magnetic, and optical properties of cubic $NdInO_3$. The exchange correlation potential has been solved by Perdew–Burke–Ernzerhof generalized gradient approximation (PBE + GGA) [26]. Nd ($4f^4\ 6s^2$), In ($4d^{10}\ 5s^2\ 5p^1$), and O ($2s^2\ 2p^4$) are taken as valence orbitals. The core of the potential well is divided into two regions: muffin-tin and interstitial region. The solution of wave function I in the muffin-tin region is considered spherical harmonic type and in II interstitial region plane wave like. The muffin-tin radii (R_{MT}) are always selected such that leakage current from the core must be zero and total energy converges. The values of R_{MT} for Nd, In, and O are taken to be 2.5, 1.75, and 1.75 (bohr), respectively. $R_{MT}K_{max} = 9$ are taken as plan wave parameters, where R_{MT} is the minimum value of muffin-tin radius and K_{max} is the highest value of K vector modulus for the plan wave in the first Brillouin zone. The k-mesh has been selected by iteration process for the best convergence and the order of k-mesh as $10 \times 10 \times 10$. The input parameters G_{max} and k points are taken as 12 and 1000, respectively, in irreducible Brillouin zone; further, − 6.0 Ryd is chosen as threshold energy for separating the valance and core states. Herein, Charpin's method [27] is used to figure out the elastic constants which further employed to estimate the mechanical parameters.

3 Results and Discussion

3.1 Structural Properties

In this study, the structure of cubic perovskite $NdInO_3$ (space group Pm3m) has been investigated, where the atoms in a unit cell are positioned at Nd (0, 0, 0), In (1/2, 1/2, 1/2) and O (0, 1/2, 1/2), (1/2, 0, 1/2), (1/2, 1/2, 0) locations. The crystal structure of the cubic $NdInO_3$ is analyzed using full potential linearized augmented plan wave as implemented in WIEN2k package by PBE-GGA approximation. The structural and geometric optimization is achieved by determining the total energy per unit cell versus volume of the compound; additionally, lattice constant and other optimized structural parameters are obtained by fitting the Murnaghan equation into total energy versus volume plots [28].

$$E(V) = a + Vb^{-2/3} + cV^{-3/4} + \mathrm{d}V^{-6/3} \tag{1}$$

Here, a, b, c, and d are the fitting parameters at the equilibrium and V represents the unit cell volume. Figure 1a shows optimized energy versus volume plots of paramagnetic and ferromagnetic states of cubic perovskite $NdInO_3$; Fig. 1b shows cubic structure of $NdInO_3$. The ferromagnetic state has lower energy than paramagnetic phase; hence, the thermodynamically more stable configuration is ferromagnetic state.

Moreover, the calculated optimized structural parameters like lattice constant, bulk modulus, and its pressure derivative, and ground state energy are given in Table 1. The lattice constant is analytically estimated via ionic radii method using the following relation [29].

$$a_0 = \alpha + \beta(r_{Nd} + r_O) + \gamma(r_{In} + r_O) \tag{2}$$

where values of α, β, and γ are 0.06741, 0.4905, and 1.2921, respectively, while r_{Nd} is ionic radii of Nd (0.995 Å), r_{In} is ionic radii of In (0.8 Å), and r_O is ionic radii of O (1.4 Å). The calculated lattice constant from PBE-GGA is in good agreement with the experimentally and analytically determined lattice constant of cubic $NdInO_3$ compound (Table 1). The bond lengths are crucial parameters to determine the tolerance factor (t) which is related to the stability of crystal structure of a particular compound. Bond length method (also known as Goldschmidt method) [30] represented by Eq. (2) and ionic radii [29] method are used to evaluate the tolerance factor.

$$t = \frac{0.707(\langle \mathrm{A} - \mathrm{O} \rangle)}{(\langle \mathrm{B} - \mathrm{O} \rangle)} \tag{3}$$

$$t = \frac{0.707(r_A + r_O)}{(r_B + r_O)} \tag{4}$$

⟨A–O⟩ denotes bond length of Nd–O and ⟨B–O⟩ of In–O. The tolerance factor (t) is a measure of any deviation from the ideal cubic structure. Usually, the tolerance factor (t) of cubic perovskites takes values in the range 0.93–1.04 [31, 32] and calculated value of tolerance factor ($t = 0.99$) of studied material lies in this range; hence, the material is stable in the cubic phase.

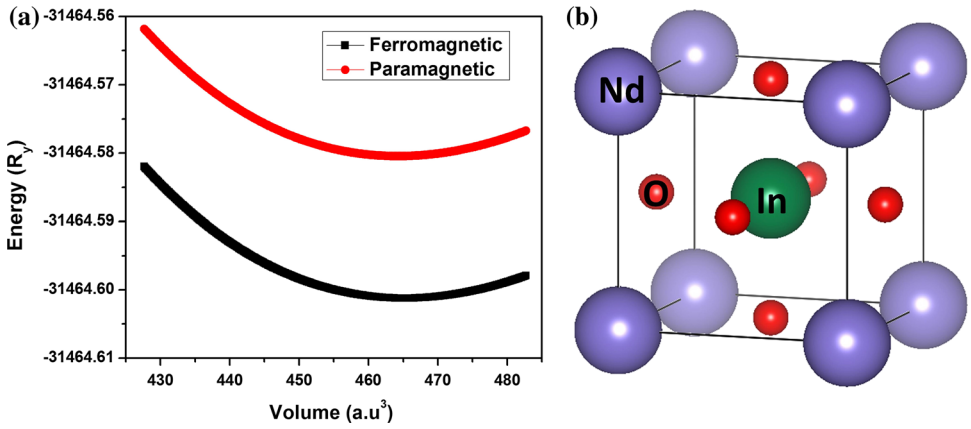

Fig. 1 **a** Optimized energy versus volume plots of paramagnetic and ferromagnetic states of cubic perovskite $NdInO_3$. **b** The cubic structure of $NdInO_3$

Table 1 Calculated values of lattice constant (a_0), bulk modulus, pressure derivative of bulk (B'), tolerance factor, and ground state energies of stable state of cubic $NdInO_3$

Parameters	Present work	Analytical	Experimental work	Previous work
Lattice constant (Å)	4.09	4.08	4.07[a]	3.99[b]
Bulk modulus (GPa)	157.1			
B'	5.00			
Volume (a.u.)^3	465.200			
E_0 (Ry)	− 31,464.601			
Tolerance factor (t)	0.99	0.98		
Bond length				
Nd–O	2.89			
Nd–In	3.54			
In–O	2.05			

[a][33]
[b][34]

3.2 Electronic and Magnetic Properties

The spin-polarized electronic band structure (BS) and density of states (DOS) of stable ferromagnetic state calculated from PBE-GGA along the high symmetry axis of irreducible Brillouin zone are depicted in Fig. 2a–c. The Fermi level (E_F) is set to 0 eV. Figure 2 shows that $NdInO_3$ is metallic in spin-up version due to the crossing of Nd-*f* states from valence to conduction bands across the Fermi level, while these states are shifted toward the conduction band resulting in semiconducting character in spin-down state. This variation of band gap in spin-up and spin-down channels proves the half metallic nature of cubic $NdInO_3$. Moreover, the TDOS (Fig. 2b) and the BS (Fig. 2 a, c) plots illustrate the same band gap that enhance the reliability of the presented results. The calculated band gap is 1.99 eV.

In order to understand the effect of individual orbitals on DOS, spin-polarized partial density of states (PDOS) is plotted in Fig. 3. However, the PDOS is divided into three distinct regions, namely lower and upper valence bands, and conduction band. The lower valence band stretching from − 14 to − 5 eV is mainly populated by In-4*d* states, inclusive of feeble contribution from O-2*s* and O-2*p* atoms, while the upper valence band extending from − 5 eV to E_F is primarily occupied by 2*p* states of O with admixture of In-4*d* and In-4*p* atoms from both spin channels (up and down). Similarly, the conduction band extends from 4.5 to 14 eV is occupied by Nd-4*p*, and slight participation of O-2*p* states for both channels. It is noted that hybridized states of Nd-4*f* and O-2*p* cross the Fermi level in case of spin-up electrons while the Nd-4*f* state is located in the range of + 2 and + 3 eV for spin-down channel (Fig. 3). Hence, the half metallic ferromagnetic nature of $NdInO_3$ compound is a result of Nd-4*f* and very small contribution of O-2*p* states. Similar type of half metallic ferromagnetic property originated due to 4*f* states which has been reported earlier in $NdGaO_3$ and $EuAlO_3$ [14, 22].

The individual, total and interstitial magnetic moments were computed by PBE-GGA approximation. This was done for all atoms at various sites of cubic $NdInO_3$ cell in order to determine the possible origin of magnetism and influence of different spins on this compound; the outcomes of these entities are summarized in Table 2. It is noted that the maximum magnetization arises from Nd site while minor magnetism originates from the feeble hybridization between the non-magnetic O-2*p* and In-4*d* states. The total magnetic moment

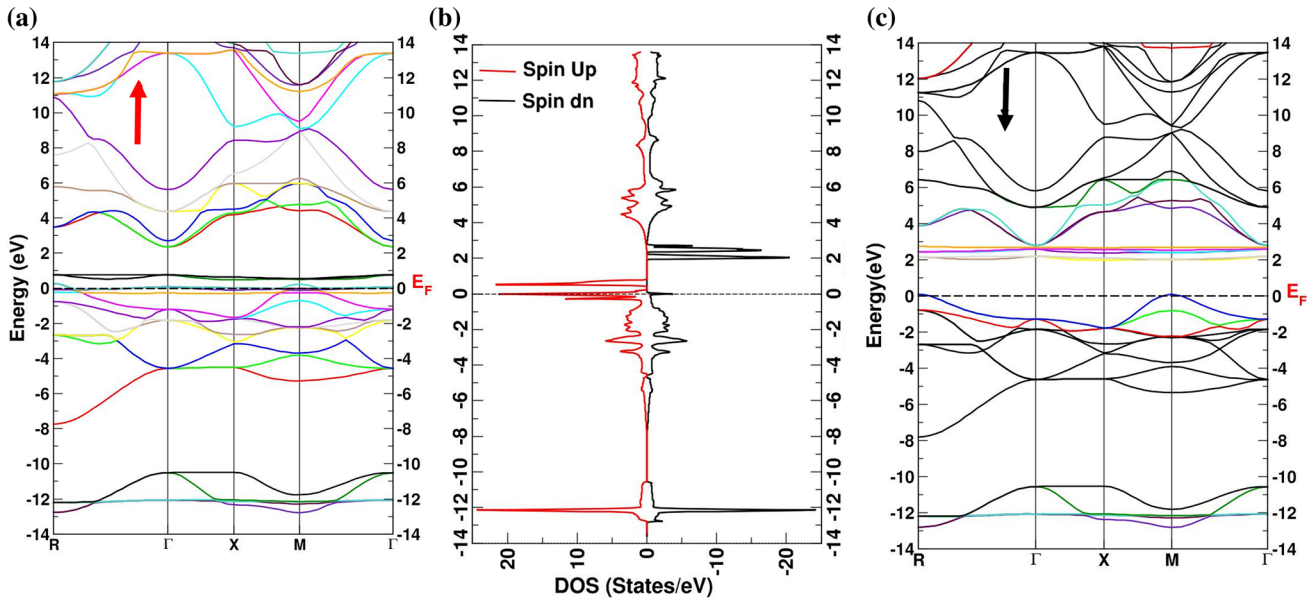

Fig. 2 **a**, **c** Spin-polarized PBE-GGA calculated band structure and **b** total density of states of cubic $NdInO_3$ in ferromagnetic phase (spin-up (↑) and spin-down (↓))

(μ_{total}) of cubic $NdInO_3$ perovskite is 3 μB, indicating its half metallic ferromagnetic nature, as the integer values of magnetic moments corresponds to the half metallic character of the material.

Furthermore, the sign of magnetic moments of the different atoms indicates the direction of spin alignment. A positive magnetic moment of different atoms illustrates that the spins align in the same direction, while a negative sign reveals ferromagnetic or anti ferromagnetic interaction. The magnetic moment of Nd and O, and In has opposite signs, which is an evidence that spins of Nd, O and In atoms interact in ferrimagnetic coder. Consequently, it is well established from density of states and magnetic outcomes that cubic $NdInO_3$ compound is a half metallic ferromagnetic.

3.3 Elastic Properties

The stability of structure and elastic properties of cubic $NdInO_3$ has been determined from the elastic stiffness constants C_{kl}. However, due to cubic structure of $NdInO_3$ only three independent elastic constants are estimated, by executing the Charpin's method within WIEN2k package. These elastic constants fulfill the mechanical stability conditions ($C_{44} > 0$); ($C_{11} > 0$); ($C_{11} - C_{12}) > 0$; ($C_{11} + 2C_{12}) > 0$, and cubic stability criteria ($C_{11} < B < C_{44}$) [35–37]. The smallest value of C_{12} indicates that this material is more easily compressed along C_{12} direction as compared to other directions. Furthermore, Voigt–Reuss–Hill approximation [38–40] is used to analyze the polycrystalline behavior from values of elastic constants of single crystal. Voigt's shear modulus (G_v) and Reuss's shear modulus (G_R) are averaged to figure out Hill shear modulus (G). The shear modulus describes the crystal strength against the shearing strain or plastic deformation. The higher values of shear modulus correspond to covalent bonded materials. The bulk and Young's moduli are derived from the elastic constants [41, 42].

$$G_R = \frac{5C_{44}(C_{11} - C_{12})}{4C_{44} + 3(C_{11} - C_{12})} \tag{5}$$

$$G_V = \frac{1}{5}(C_{11} - C_{12} + 3C_{44}) \tag{6}$$

$$G = \frac{G_V + G_R}{2} \tag{7}$$

$$B = \frac{C_{11} + 2C_{12}}{3} \tag{8}$$

$$Y = \frac{9G_v}{G_v + 3B} \tag{9}$$

Moreover, the rigidity of the material is associated with the bulk modulus. The higher obtained values of the bulk modulus illustrate the incompressible nature of $NdInO_3$. Similarly, Young's modulus is another parameter to check the stiffness of the material, and hard and covalent bonded materials have higher values of Young's modulus. Therefore, the calculated values of Young's modulus, shear modulus, and bulk modulus clearly indicate rigid and covalent behavior of the materials (Table 3). In addition, the ductile and brittle nature of the $NdInO_3$ is verified by the Pugh's (B/G) and Poisson's ratios $\upsilon = \frac{3B-2G}{2(3B+G)}$. The cutoff values of Pugh's ratio are 1.75 and Poisson's ratio are 0.26. When the $B/G > 1.75$ and $\upsilon \geq 0.26$, the material exhibits ductile character; otherwise, it shows brittle nature [43, 44]. The Poisson's ratio is 0.23 and

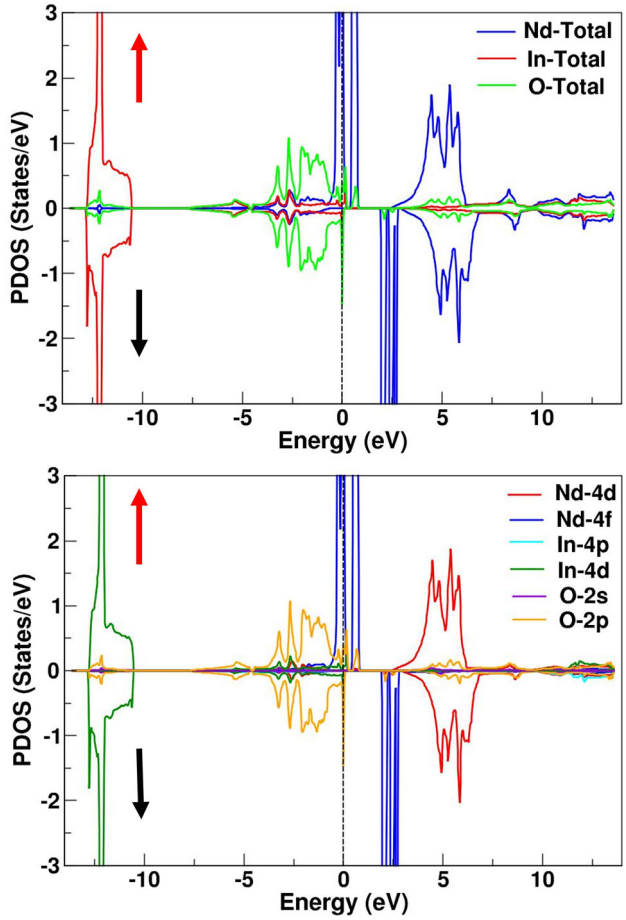

Fig. 3 Spin-polarized partial density of states (PDOS) of $NdInO_3$ at equilibrium lattice parameters by PBE-GGA

Table 2 Calculated total, interstitial, and individual atomic magnetic moments (μ_B) of cubic $NdInO_3$

Compound	Total	Interstitial	Nd	In	O
$NdInO_3$	3.000	0.100	3.174	− 0.014	− 0.086

Pugh's ratio is 1.51 which reveals the brittle nature of this compound (Table 2). Last but not least, anisotropic factor is a very important factor to determine the isotropic (amorphous) and anisotropic (crystalline) property of the material. The calculated anisotropic value of $NdInO_3$ ($A = 0.39$) designates this material as anisotropic. Material with $A = 1$ established isotropic nature and any deviation from 1 signifies anisotropic behavior [45]. Henceforth, the overall elastic properties of $NdInO_3$ justify the rigid, brittle, and anisotropic nature of this material.

$$A = \frac{2C_{44}}{C_{11} - C_{44}} \tag{10}$$

3.4 Optical Properties

The optical properties can be explained in terms of reflection, polarization, dispersion, conduction, and absorption. The complex dielectric function explains the dispersion and absorption of the external electromagnetic radiations which are schematically represented in Fig. 4a and b. The band structure and dielectric function are directly linked with each other which increased the importance of this function, while revealing the optical characteristics of the material. The dielectric function consists of real and imaginary part. The imaginary part ε_2 (ω) exhibits material's capability for absorption of energy and calculated by direct transition from valence to conduction band. The values of ε_2 (ω) are taken from energy range 0–14 eV. The highest peak at 5.5 eV shows the maximum absorption of incident light in ultraviolet region of spectrum. The broad absorption region extending from 3.7 to 9.7 eV indicates that this material could be applied in the optical devices that work in the ultraviolet range.

The real part of complex dielectric function ε_1 (ω) expresses the polarization of incident light and can be derived from the ε_2 (ω) by means of Kramers–Krong relation [46]. A schematic of the real part is given in Fig. 4a. Herein, ε_1 (ω) linearly increases with energy and reaches a maximum value at 4.3 eV, and after some attenuations its value becomes negative in the 6–7 eV region and negative values correspond to the metallic behavior. Moreover, the band gap and zero frequency limit of the studied material also fulfill Penn's mode $\varepsilon_1(0) \approx 1 + (\hbar\omega_p/E_g)^2)$ [47]. The refractive index n (ω) and extinction coefficient k (ω) are related to the real and imaginary part by $n^2 - k^2 = \varepsilon_1$ (ω) and $2nk = \varepsilon_2$ (ω), respectively. The pattern of n (ω) is analogous to ε_1 (ω) and k (ω) to ε_2 (ω) [48]. The refractive index is an important factor to find the potential application of different materials in optoelectronic equipment. It describes the transparency of the materials when light falls on their surface. If the material is highly transparent, the value of refractive index becomes very low (approximately zero) and the positive values indicate the absorption of light by the material. The zero frequency limit of refractive index satisfies the relation $n^2(0) = \varepsilon_1$ (ω), a further rise in energy leads to an increase in transparency, and the maximum value lies in 3.3–6.2 eV energy range as demonstrated in Fig. 4b. Additionally, k (ω) describes the capability of the material to absorb light. The studied material shows sharp peaks within 3.8–10 eV (Fig. 4b). Reflectivity is another important parameter for optoelectronics and is defined as a ratio between incident and reflected light. The value of reflectivity rises from zero frequency limit R (0) and changes with energy as illustrated in Fig. 4c.

The values of reflectivity are at their maximum when the absorption values are at their minimum. The frequency-dependent absorption coefficient is shown in Fig. 5a. The sharp peaks of absorption coefficient appear between 20 and

Table 3 Calculated elastic constant, Young's modulus (Y), anisotropy (A), shear modulus (G), bulk modulus (B), and Poisson's ratio (ν) of cubic perovskite $NdInO_3$ using PBE + GGA approximation

C_{11}	C_{12}	C_{44}	B	A	G	G_v	G_R	Y	ν	B/G
426.20	27.40	78.61	159.34	0.39	99.62	95.48	103.75	239.00	0.25	1.61

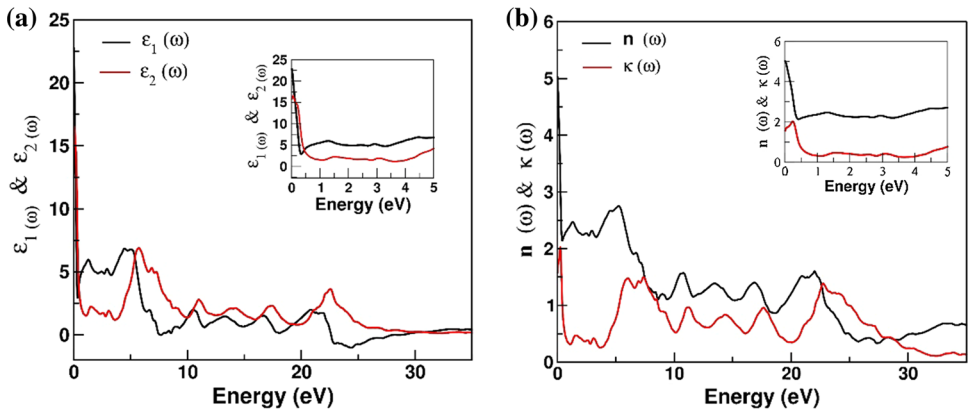

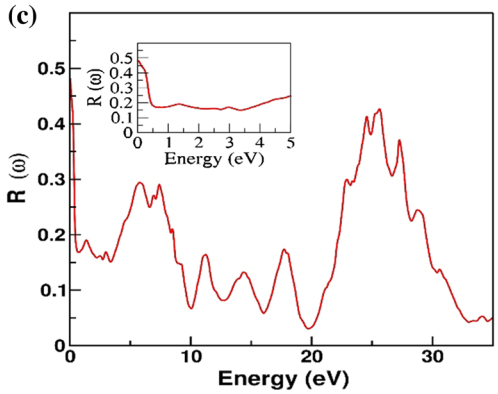

Fig. 4 Plots of **a** complex dielectric constants, **b** refractive index and extinction coefficient, **c** reflectivity computed for stable state of $NdInO_3$

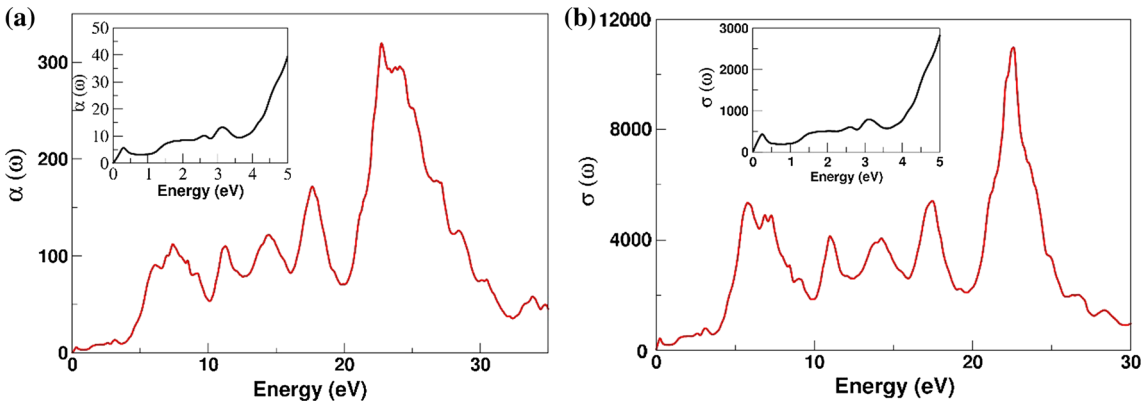

Fig. 5 Plots of **a** absorption coefficient and **b** optical conductivity, computed for stable state of $NdInO_3$

29.7 eV, which discloses the suitability of this material for optoelectronic devices. The optical conductivity accounts for the free charge carriers produced as a result of bond breaking due to the electron–photon interaction. The higher absorption of light leads to the higher values of optical conductivity because photons provide more energy to break the bond. The optical conductivity has its largest peak at 22 eV with a magnitude of 11,096 $(\Omega\ \mathrm{cm})^{-1}$ as depicted in Fig. 5b.

4 Conclusion

We studied the structural, electronic, ferromagnetic, elastic, and optical properties of cubic $NdInO_3$ in detail. A PBE-GGA scheme based on DFT was used. The outcomes of this study are summarized as follows

1. The calculated lattice constants are in good agreement with analytical values and experiment.
2. The total energies demonstrate that the ferromagnetic state is energetically more stable state than paramagnetic phase.
3. The electronic properties exhibit half metallic ferromagnetic nature of cubic $NdInO_3$, which may make this compound a candidate in spintronics.
4. The elastic characteristics suggest a brittle and anisotropic nature of this material.
5. The value of the magnetic moments confirms a half metallic ferromagnetic behavior. Furthermore, we find that the main source of the magnetization is the Nd atoms.
6. This material may be suitable for ultraviolet–optical–devices due to broad absorption range in the ultraviolet region.

Acknowledgements The author (M. Yaseen) is thankful to Higher Education Commission (HEC) of Pakistan for funding through Project No: 6410/Punjab/NRPU/R&D/HEC/2016.

References

1. De Groot, R.A.; Mueller, F.M.; Van Engen, P.G.; Buschow, K.H.J.: New class of materials: half-metallic ferromagnets. Phys. Rev. Lett. **50**(25), 2024 (1983)
2. Itoh, H.; Ohsawa, T.; Inoue, J.: Magnetoresistance of ferromagnetic tunnel junctions in the double-exchange model. Phys. Rev. Lett. **84**(11), 2501 (2000)
3. Schwarz, K.: CrO_2 predicted as a half-metallic ferromagnet. J. Phys. F: Met. Phys. **16**(9), L211 (1986)
4. Bristowe, N.C.; Varignon, J.; Fontaine, D.; Bousquet, E.; Ghosez, P.: Ferromagnetism induced by entangled charge and orbital orderings in ferroelectric titanate perovskites. Nat. Commun. **6**(1), 1–6 (2015)
5. Wolf, S.A.; Awschalom, D.D.; Buhrman, R.A.; Daughton, J.M.; von Molnár, V.S.; Roukes, M.L.; Chtchelkanova, A.Y.; Treger, D.M.: Spintronics: a spin-based electronics vision for the future. Science **294**(5546), 1488–1495 (2001)
6. Pickett, W.E.; Moodera, J.S.: Half metallic magnets. Phys. Today **54**(5), 39–45 (2001)
7. Millis, A.J.: Electron-lattice coupling in "colossal" magnetoresistance rare earth manganites. J. Appl. Phys. **81**(8), 5502–5503 (1997)
8. Reshak, A.H.: Specific features of electronic structures and optical susceptibilities of molybdenum oxide. RSC Adv. **5**(28), 22044–22052 (2015)
9. Frederikse, H.P.R.; Thurber, W.R.; Hosler, W.R.: Electronic transport in strontium titanate. Phys. Rev. **134**(2A), A442 (1964)
10. Schneemeyer, L.F.; Waszczak, J.V.; Zahorak, S.M.; Van Dover, R.B.; Siegrist, T.: Superconductivity in rare earth cuprate perovskites. Mater. Res. Bull. **22**(11), 1467–1473 (1987)
11. Sheikh, M.S.; Sakhya, A.P.; Maity, R.; Dutta, A.; Sinha, T.P.: Narrow band gap and optical anisotropy in double perovskite oxide Sm_2NiMnO_6: a new promising solar cell absorber. Sol. Energy Mater. Sol. Cells **193**, 206–213 (2019)
12. Moritomo, Y.; Asamitsu, A.; Kuwahara, H.; Tokura, Y.: Giant magnetoresistance of manganese oxides with a layered perovskite structure. Nature **380**(6570), 141–144 (1996)
13. Teresa, J.D.; Ibarra, M.R.; Algarabel, P.A.; Ritter, C.; Marquina, C.; Blasco, J.; Garcia, J.; Moral, A.D.; Arnold, Z.: Evidence for magnetic polarons in the magnetoresistive perovskites. Nature **386**(6622), 256–258 (1997)
14. Monir, M.E.A.; Baltach, H.; Hassan, F.E.H.; Bahnes, A.; Bahnes, Z.: Study of structural, electronic, and magnetic properties of cubic lanthanide based on oxide perovskite-type $NdGaO_3$. J. Supercond. Nov. Magn. **32**(7), 2149–2154 (2019)
15. Bouadjemi, B.; Bentata, S.; Abbad, A.; Benstaali, W.; Bouhafs, B.: Half-metallic ferromagnetism in $PrMnO_3$ perovskite from first principles calculations. Solid State Commun. **168**, 6–10 (2013)
16. Liu, Y.P.; Fuh, H.R.; Wang, Y.K.: First-principles study of half-metallic materials in double-perovskite A_2FeMO_6 (M = Mo, Re, and W) with IVA group elements set on the A-site position. J. Phys. Chem. C **116**(34), 18032–18037 (2012)
17. Monir, M.E.A.; Baltache, H.; Murtaza, G.; Khenata, R.; Ahmed, W.K.; Bouhemadou, A.; Omran, S.B.; Seddik, T.: Spin-polarized structural, elastic, electronic and magnetic properties of half-metallic ferromagnetism in V-doped ZnSe. J. Magn. Magn. Mater. **374**, 50–60 (2015)
18. Xie, W.H.; Liu, B.G.: Half-metallic ferromagnetism in ternary transition-metal compounds based on ZnTe and CdTe semiconductors. J. Appl. Phys. **96**(6), 3559–3561 (2004)
19. Kobayashi, K.I.; Kimura, T.; Sawada, H.; Terakura, K.; Tokura, Y.: Room-temperature magnetoresistance in an oxide material with an ordered double-perovskite structure. Nature **395**(6703), 677–680 (1998)
20. Park, J.H.; Vescovo, E.; Kim, H.J.; Kwon, C.; Ramesh, R.; Venkatesan, T.: Magnetic properties at surface boundary of a half-metallic ferromagnet $La_{0.7}Sr_{0.3}MnO_3$. Phys. Rev. Lett. **81**(9), 1953 (1998)
21. Rashid, M.; Abbas, Z.; Yaseen, M.; Afzal, Q.; Mahmood, A.; Ramay, S.M.: Theoretical investigation of cubic $BaVO_3$ and $LaVO_3$ Perovskites via Tran–Blaha-Modified Becke–Johnson exchange potential approach. J. Supercond. Nov. Magn. **30**(11), 3129–3136 (2017)
22. Sandeep, C.; Rai, D.P.; Shankar, A.; Ghimire, M.P.; Khenata, R.; Thapa, R.K.: Study of electronic and magnetic properties in 4f electron based cubic $EuAlO_3$: a first-principles calculation. Phys. Scr. **90**(6), 065803 (2015)
23. Li, D.; Luo, C.; Wang, H.: Effects of pressure on the structural, electronic, and optical properties of rhombohedral $NdAlO_3$: Ab initio study. Ferroelectrics **520**(1), 144–153 (2017)
24. Yang, C.Y.; Zhang, R.; Zhang, L.M.; Ke, X.W.: Electronic structure and optical properties of 0.5 $NdAlO_3$-0.5 $CaTiO_3$ from first-principles calculation. Acta Phys. Sin. **61**, 77702 (2012)
25. Blaha, P.; Schwarz, K.; Sorantin, P.; Trickey, S.B.: Full-potential, linearized augmented plane wave programs for crystalline systems. Comput. Phys. Commun. **59**(2), 399–415 (1990)
26. Perdew, J.P.; Burke, K.; Ernzerhof, M.: Generalized gradient approximation made simple. Phys. Rev. Lett. **77**(18), 3865 (1996)
27. Blaha, P.; Schwarz, K.; Madson, G.; Kvasnicka, D.; Luitz, J.: User's Guide, WIEN2k Vienna University of Technology, Austria (2010)
28. Murnaghan, F.D.: The compressibility of media under extreme pressures. In: 1944 Proceedings of the National Academy of Sciences of the United States of America, vol. **30**, no. 9, pp. 244–247 (1944)

29. Ubic, R.: Revised method for the prediction of lattice constants in cubic and pseudocubic perovskites. J. Am. Ceram. Soc. **90**(10), 3326–3330 (2007)
30. Goodenough, J.B.: Electronic and ionic transport properties and other physical aspects of perovskites. Rep. Prog. Phys. **67**(11), 1915 (2004)
31. Li, Z.; Yang, M.; Park, J.S.; Wei, S.H.; Berry, J.J.; Zhu, K.: Stabilizing perovskite structures by tuning tolerance factor: formation of formamidinium and cesium lead iodide solid-state alloys. Chem. Mater. **28**(1), 284–292 (2016)
32. Xu, N.; Zhao, H.; Zhou, X.; Wei, W.; Lu, X.; Ding, W.; Li, F.: Dependence of critical radius of the cubic perovskite ABO_3 oxides on the radius of A-and B-site cations. Int. J. Hydrog. Energy **35**(14), 7295–7301 (2010)
33. Geguzina, G.A.; Sakhnenko, V.P.: Correlation between the lattice parameters of crystals with perovskite structure. Crystallogr. Rep. **49**(1), 15–19 (2004)
34. Verma, A.S.; Jindal, V.K.: Lattice constant of cubic perovskites. J. Alloys Compd. **485**, 514–518 (2009)
35. Gupta, D.C.; Bhat, I.H.: Full-potential study of Fe_2NiZ (Z = Al, Si, Ga, Ge). Mater. Chem. Phys. **146**(3), 303–312 (2014)
36. Wang, J.; Yip, S.; Phillpot, S.R.; Wolf, D.: Crystal instabilities at finite strain. Phys. Rev. Lett. **71**(25), 4182 (1993)
37. Ghimire, M.P.; Sinha, T.P.; Thapa, R.K.: First principles study of the electronic and magnetic properties of semi-Heusler alloys NiXSb (X = Ti, V, Cr and Mn). J. Alloys Compd. **509**(41), 9742–9752 (2011)
38. Voigt, W.: On the relation between the elasticity constants of isotropic bodies. Ann. Phys. Chem. **274**, 573–587 (1889)
39. Reuß, A.: Calculation of the flow limit of mixed crystals due to the plasticity condition for single crystals. J. Appl. Math. Mech. **9**(1), 49–58 (1929)
40. Hill, R.: The elastic behaviour of a crystalline aggregate. Proc. Phys. Soc. Sect. A **65**(5), 349 (1952)
41. Yousuf, S.; Gupta, D.C.: Investigation of electronic, magnetic and thermoelectric properties of Zr_2NiZ (Z = Al, Ga) ferromagnets. Mater. Chem. Phys. **192**, 33–40 (2017)
42. Dieter George, E: Mechanical Metallurgy. SI metric edition. McGraw-Hili Book Company, London, p. 669 (1988)
43. Pugh, S.F.: XCII. Relations between the elastic moduli and the plastic properties of polycrystalline pure metals. Lond Edinburgh Dublin Philos Mag J Sci **45**(367), 823–843 (1954)
44. Frantsevich, I.N.; Voronov, F.F.; Bokuta, S.A.: Elastic Constants and Elastic Moduli of Metals and Insulators Handbook; Frantsevich, I.N, Naukova Dumka (Kiev, Ukraine) p. 80 (1983)
45. Chauhan, M.; Gupta, D.C.: Electronic, mechanical, phase transition and thermo-physical properties of TiC, ZrC and HfC: high pressure computational study. Diam. Relat. Mater. **40**, 96–106 (2013)
46. Marius, G.: The Physics of Semiconductor, 2nd edn, p. 76. Springer, Berlin (2010)
47. Penn, D.R.: Wave-number-dependent dielectric function of semiconductors. Phys. Rev. **128**(5), 2093 (1962)
48. Khenata, R.; Sahnoun, M.; Baltache, H.; Rérat, M.; Rashek, A.H.; Illes, N.; Bouhafs, B.: First-principle calculations of structural, electronic and optical properties of $BaTiO_3$ and $BaZrO_3$ under hydrostatic pressure. Solid State Commun. **136**(2), 120–125 (2005)